PHYSICAL REVIEW D **88,** 104025 (2013)

Black hole remnant of black hole-neutron star coalescing binaries

Francesco Pannarale*

Max-Planck-Institut für Gravitationsphysik, Albert Einstein Institut, Potsdam, Germany
and School of Physics and Astronomy, Cardiff University, The Parade, Cardiff CF24 3AA, United Kingdom

(Received 5 September 2012; published 22 November 2013)

We present a model for determining the dimensionless spin parameter and mass of the black hole remnant of black hole-neutron star mergers with parallel orbital angular momentum and initial black hole spin. This approach is based on the Buonanno, Kidder, and Lehner method for binary black holes, and it is successfully tested against the results of numerical-relativity simulations: the dimensionless spin parameter is predicted with absolute error $\lesssim 0.02$, whereas the relative error on the final mass is $\lesssim 2\%$, its distribution in the tests being pronouncedly peaked at 1%. Our approach and the fit to the torus remnant mass reported in [57] thus constitute an easy-to-use analytical model that accurately describes the remnant of black hole-neutron star mergers. The space of parameters consisting of the binary mass ratio, the initial black hole spin, and the neutron star mass and equation of state is investigated. We provide indirect support to the cosmic censorship conjecture for black hole remnants of black hole-neutron star mergers. We show that the presence of a neutron star affects the quasinormal mode frequency of the black hole remnant, thus suggesting that the ringdown epoch of the gravitational wave signal may virtually be used to (1) distinguish black hole-black hole from black hole-neutron star mergers and to (2) constrain the neutron star equation of state.

DOI: 10.1103/PhysRevD.88.104025 PACS numbers: 04.30.Db, 04.25.dk, 95.30.Sf, 97.60.Jd

I. INTRODUCTION

Once a black hole-neutron star (BH-NS) binary is formed, gravitational radiation reaction gradually reduces its orbital separation until the two companions merge and leave behind a remnant consisting of a black hole and, possibly, a hot, massive accretion torus surrounding it [1]. BH-NS binaries have not been observed yet; population synthesis studies, however, suggest that the coalescence of BH-NS systems is likely to occur frequently in the Hubble volume, thus making theoretical studies on the evolution and final state of BH-NS mergers relevant [2–6]. Interest in these systems arises from the fact that they are among the most promising sources for gravitational wave (GW) detectors—such as LIGO [7], Virgo [8], KAGRA [9], and the Einstein Telescope [10]—and that they are promising candidates as progenitors of (a fraction of) short-hard gamma-ray bursts [11,12]. Further, as NSs in these systems undergo strong tidal deformations, observing GW and/or electromagnetic signals emitted by BH-NS binaries could help shed light on the equation of state (EOS) of matter at supranuclear densities, which is currently unknown [13–16]. Finally, comprehending the fate of the material possibly ejected by BH-NS binaries after the NS tidal disruption is relevant in interpreting the observed abundances of the heavy elements that are formed by rapid neutron capture in *r*-processes [17]. These outflows may additionally be observable due to the radioactive decays triggered by the formation of heavy isotopes, i.e. "kilonovas," or due to the shock they would generate when hitting interstellar medium of sufficiently high density [18].

To achieve a full understanding of BH-NS merger events and their physics, numerical-relativity simulations are required. These will ultimately have to include adequate and accurate treatments of general relativity, relativistic (magneto)hydrodynamics, the microphysical EOS, NS crust physics, thermal effects, and nuclear physics reactions. Numerical quasiequilibrium studies [19–25] and dynamical simulations [16,26–55] of mixed binary mergers made considerable progress in the last few years. Despite the fact that simulating BH-NS mergers is now possible, these simulations remain nevertheless both challenging and computationally intensive. This has motivated the parallel development of pseudo-Newtonian BH-NS calculations, e.g. [56], and analytical approaches focusing on specific physical aspects of the problem, e.g. [13–15,57–64]. Studies of these kinds benefit from their low computational costs, which allow them to shed light on questions that cannot be currently addressed with numerical simulations and to provide insight on what happens when the large space of parameters of BH-NS binaries is spanned. They may, in turn, aid numerical relativity by suggesting cases that are particularly interesting to simulate and by providing information to exploit within the simulations themselves.

In this paper we focus on predicting the spin parameter and mass of the BH remnant of BH-NS coalescing binaries by using a semianalytical approach. While this problem has a fairly long history in the case of coalescing binary black holes [65–85], no attempt beyond numerical-relativity simulations has yet been made to tackle it in the case of BH-NS mergers. The approach we present and discuss is based on the work of Buonanno, Kidder, and Lehner (BKL) on estimating the final BH spin of a coalescing binary BH with arbitrary initial masses and spins [74]. We choose this simple,

*francesco.pannarale@aei.mpg.de

phenomenological model as a starting point because it provides good physical insight and because it is straightforward to modify and extend. Our method may indeed be seen as a generalization of the BKL model to the case in which the lower mass BH is replaced with a NS. For the time being, however, it is restricted to systems in which the BH spin direction is parallel to the orbital angular momentum direction. The closed expression we determine for the final spin parameter automatically yields an estimate of the mass of the BH remnant by means of a method similar to the starting point of Barausse, Morozova, and Rezzolla's calculations on the mass radiated by binary BHs [85], but with modifications inspired, once again, by [74]. The key equations of our approach are Eqs. (9), (11), and (12) and, despite the mathematical complexity of the mixed binary coalescence problem, our method enables us to reproduce the results of numerical-relativity simulations with reasonable accuracy.

The paper is organized as follows. In Sec. II we review the BKL approach for binary BHs. In Sec. III we propose an extension of this method in order to predict the spin parameter and mass of BH remnants of BH-NS mergers—Eqs. (9), (11), and (12)—and successfully test it against available numerical-relativity data. In Sec. IV we gather the results obtained by systematically varying the binary mass ratio, the initial BH spin parameter, and the NS mass and EOS. First, we provide indirect support to the cosmic censorship conjecture and suggest particularly interesting cases to explore with numerical simulations in this context (Sec. IV A). Then, we show that the NS EOS may leave an imprint on the BH remnant in terms of its final spin and mass (Sec. IV B). This suggests the idea of inferring the presence of the NS and of constraining its EOS from the ringdown of the BH remnant. Finally, in Sec. V, we draw our conclusions and collect our remarks.

II. THE BKL FORMULA

The BKL approach to estimate the final spin of BH-BH mergers [74] starts by considering an initial reference state with two widely separated black holes approximated as two Kerr black holes having masses $\{M_1, M_2\}$ and dimensionless spin parameters[1] $\{a_1, a_2\}$. The case of the BKL approach that we will extend in order to describe BH-NS binaries is that of BH binary systems, the orbits of which stay within a unique plane, referred to as the equatorial plane; in such cases, the orbital angular momentum and the individual spins of the BHs are orthogonal to the equatorial plane. The spin parameter of the BH remnant $a_{\rm f}$ is obtained in terms of the initial configuration of the system by a phenomenological approach that relies on the following two observations based on intuitive arguments, on post-Newtonian and perturbative calculations for the inspiral and ringdown, and on numerical simulations of the merger:

(1) The system evolves quasiadiabatically during the inspiral phase.
(2) The total mass and angular momentum of the system change only by a small amount during the merger and ringdown phases.

Further, the BKL expression for $a_{\rm f}$ is derived from first principles once the following assumptions are made:

(1) The mass of the system is conserved to first order, so that the *final* BH has a total mass $M = M_1 + M_2$.
(2) The magnitude of the individual BH spins remains constant, and their contribution to the final total angular momentum is determined by the their initial values.
(3) The system radiates much of its angular momentum in the long inspiral stage until it reaches the innermost stable circular orbit (ISCO), when the dynamics quickly leads to the merger of the two BHs. Given that the radiation of energy and angular momentum during the merger is small with respect to the mass and angular momentum of the system, the contribution of the orbital angular momentum to the angular momentum of the BH remnant is estimated by considering the orbital angular momentum of a test particle orbiting a Kerr BH, with spin parameter equal to that of the *final* BH, at the ISCO.

All these assumptions are combined in the following formula expressing the dimensionless spin parameter of the final BH:

$$a_{\rm f} = \frac{a_1 M_1^2 + a_2 M_2^2 + l_z(\bar{r}_{\rm ISCO,f}, a_{\rm f}) M_1 M_2}{M^2}, \qquad (1)$$

where $l_z(\bar{r}_{\rm ISCO,f}, a_{\rm f})$ is the orbital angular momentum per unit mass of a test particle orbiting the BH remnant at the ISCO, and where we introduced the notation $\bar{r} = r/M$ for the (dimensionless) Boyer-Lindquist radial coordinate.

We recall that for equatorial orbits around a Kerr BH of spin parameter a,

$$l_z(\bar{r}, a) = \pm \frac{\bar{r}^2 \mp 2a\sqrt{\bar{r}} + a^2}{\sqrt{\bar{r}}(\bar{r}^2 - 3\bar{r} \pm 2a\sqrt{\bar{r}})^{1/2}}, \qquad (2)$$

and that the orbital separation at the ISCO is given by

$$\begin{aligned} \bar{r}_{\rm ISCO} &= \left[3 + Z_2 \mp \sqrt{(3 - Z_1)(3 + Z_1 + 2Z_2)}\right] \\ Z_1 &= 1 + (1 - a^2)^{1/3}[(1 + a)^{1/3} + (1 - a)^{1/3}] \\ Z_2 &= \sqrt{3a^2 + Z_1^2}, \end{aligned} \qquad (3)$$

where upper/lower signs hold for co/counter-rotating orbits. Throughout the paper we will use the symbols $\bar{r}_{\rm ISCO,i}$ and $\bar{r}_{\rm ISCO,f}$ to denote $\bar{r}_{\rm ISCO}$ calculated for the initial and final BH spin parameter, respectively. In the following, we will also be using the energy per unit mass e of a test particle orbiting a BH. It may be expressed as

[1] In [74] a's have the dimensions of a mass, while they are dimensionless throughout this paper.

$$e(\bar{r}, a) = \frac{\bar{r}^2 - 2\bar{r} \pm a\sqrt{\bar{r}}}{\bar{r}(\bar{r}^2 - 3\bar{r} \pm 2a\sqrt{\bar{r}})^{1/2}} \tag{4}$$

for Kerr equatorial orbits.

III. A MODEL FOR BH-NS MERGERS

When modifying Eq. (1) in order to describe BH-NS systems, the first step is to set the initial spin angular momentum of the NS to zero since (1) this is believed to be a reliable approximation of astrophysically realistic systems [86,87] and (2) this was done in all BH-NS merger numerical simulations so far and we use these as test cases to assess the validity of our model. Adapting the notation in Eq. (1) to BH-NS binaries, we now have

$$a_{\rm f} = \frac{a_{\rm i} M_{\rm BH}^2 + l_z(\bar{r}_{\rm ISCO,f}, a_{\rm f}) M_{\rm BH} M_{\rm NS}}{M^2}. \tag{5}$$

In the case of disruptive BH-NS mergers, an accretion torus surrounding the BH remnant may be formed, and one must thus drop assumption 1 of the BKL approach and adequately modify Eq. (5) to take this possibility into account. This is done by (1) replacing the term $l_z(\bar{r}_{\rm ISCO,f}, a_{\rm f}) M_{\rm BH} M_{\rm NS}$ in the numerator with $l_z(\bar{r}_{\rm ISCO,f}, a_{\rm f}) M_{\rm BH}(M_{\rm NS} - M_{\rm b,torus})$ and by (2) replacing M with $M - e(\bar{r}_{\rm ISCO,f}, a_{\rm f}) M_{\rm b,torus}$ in the denominator, where $M_{\rm b,torus}$ is the baryonic mass of the torus remnant. The former/latter replacement expresses the lack of angular momentum/mass accretion onto the BH due to the formation of the torus.[2] In the case of no torus formation, $M_{\rm b,torus} = 0$ and full accretion of both mass and angular momentum onto the BH is achieved. Our formula now reads

$$a_{\rm f} = \frac{a_{\rm i} M_{\rm BH}^2 + l_z(\bar{r}_{\rm ISCO,f}, a_{\rm f}) M_{\rm BH}(M_{\rm NS} - M_{\rm b,torus})}{[M - e(\bar{r}_{\rm ISCO,f}, a_{\rm f}) M_{\rm b,torus}]^2}, \tag{6}$$

where we once more emphasize that e and l_z are calculated for the ISCO and spin of the *final* BH.

A last element to take into account is that GW emission during the inspiral will further reduce the energy M that the system has at infinite orbital separation. This was not considered in the BKL model (see assumption 1 in the previous section), but we wish to include it in our extension of their formulation. It affects the denominator of Eq. (6) and may be taken into account at first order in the symmetric mass ratio $\nu = M_{\rm BH} M_{\rm NS}/(M_{\rm BH} + M_{\rm NS})^2$ by subtracting to M the additional term, e.g. [85],

$$E_{\rm rad} = M[1 - e(\bar{r}_{\rm ISCO,i}, a_{\rm i})]\nu, \tag{7}$$

so that

$$a_{\rm f} = \frac{a_{\rm i} M_{\rm BH}^2 + l_z(\bar{r}_{\rm ISCO,f}, a_{\rm f}) M_{\rm BH}(M_{\rm NS} - M_{\rm b,torus})}{[M\{1 - [1 - e(\bar{r}_{\rm ISCO,i}, a_{\rm i})]\nu\} - e(\bar{r}_{\rm ISCO,f}, a_{\rm f}) M_{\rm b,torus}]^2}. \tag{8}$$

This final, closed expression for the final spin parameter $a_{\rm f}$ may be solved numerically with root-finding techniques to determine the spin parameter of the BH remnant of BH-NS mergers, and its denominator automatically provides a prediction for the final mass of the remnant itself. In other words, once $a_{\rm f}$ is calculated, the mass of the BH remnant $M_{\rm f}$ automatically follows as

$$M_{\rm f} = M\{1 - [1 - e(\bar{r}_{\rm ISCO,i}, a_{\rm i})]\nu\} - e(\bar{r}_{\rm ISCO,f}, a_{\rm f}) M_{\rm b,torus}. \tag{9}$$

Notice that, in principle, Eq. (8) may be generalized to account for additional energy losses and for nonideal angular momentum accretion. In the former case, it is sufficient to subtract extra terms on the right-hand side of Eq. (9) and, hence, in the denominator of Eq. (8). Nonideal angular momentum accretion, which is particularly relevant for disruptive BH-NS mergers, could instead be modeled by inserting an angular momentum accretion efficiency factor in front of the l_z appearing in Eq. (8). For the time being, we keep Eq. (8) as it is, knowing that it may be improved as the nuances in the physics of BH-NS mergers become clearer.

In Tables I and II we compare the predictions of Eq. (8) and Eq. (1) to the results obtained within full general relativity in [38,43–46,48], which, along with [16,47,49–55], represent the state of the art of numerical-relativity simulations of BH-NS mergers. Each row of the tables refers to a specific BH-NS binary coalescence. The columns provide a dummy index which numbers the test cases, the reference in which the numerical-relativity results for that binary were presented, information about the NS EOS, the NS compactness $C = M_{\rm NS}/R_{\rm NS}$, the binary mass ratio $Q = M_{\rm BH}/M_{\rm NS}$, the initial BH spin parameter $a_{\rm i}$, the numerical-relativity result for the final BH spin parameter $a_{\rm f}^{\rm NR}$, the final BH spin parameter $a_{\rm f}^{\rm BKL}$ predicted by the BKL formula in Eq. (1), the final BH spin parameter $a_{\rm f,1}$ yielded by Eq. (8), and the final BH spin parameter $a_{\rm f}$ predicted by Eq. (11), which contains improvements over Eq. (8) and will be discussed later. As far as the NS EOS is concerned, the first 19 comparisons reported in Table I refer to binaries in which the nonthermal behavior of the NS matter[3] is governed, at microphysical level, by a polytropic EOS with polytropic exponent $\Gamma = 2$. In the last 18 simulations reported in Table I and in all the ones reported in Table II, on the other hand, a two-piecewise polytropic EOS was used, and the notation in the tables follows the

[2] We are introducing the approximation $L_{z,\rm torus} \equiv M_{\rm BH} \times \int_{\rm torus} d(l_z m_{\rm b}) \approx M_{\rm BH} l_z(\bar{r}_{\rm ISCO,f}, a_{\rm f}) \int_{\rm torus} d(m_{\rm b}) = M_{\rm BH} l_z \times (\bar{r}_{\rm ISCO,f}, a_{\rm f}) M_{\rm b,torus}$, and the approximation $E_{\rm torus} \equiv \int_{\rm torus} d(e m_{\rm b}) \approx e(\bar{r}_{\rm ISCO,f}, a_{\rm f}) \int_{\rm torus} d(m_{\rm b}) = e(\bar{r}_{\rm ISCO,f}, a_{\rm f}) M_{\rm b,torus}$.

[3] Here and in [57,64] thermal contributions are neglected. These are more relevant, in the merger and postmerger dynamics, when the NS is tidally disrupted.

TABLE I. Tests against numerical-relativity results. Each row is a test case numbered by the index in the first column. The remaining columns provide the reference in which the numerical-relativity simulation for the binary was presented, information about the NS EOS, the NS compactness C, the binary mass ratio Q, the initial BH spin parameter $a_{\rm i}$, and the final BH spin parameter given by the numerical-relativity simulation, $a_{\rm f}^{\rm NR}$, by the BKL approach, $a_{\rm f}^{\rm BKL}$, by Eq. (8), $a_{\rm f,1}$, and by the final formulation of our model given in Eqs. (11) and (12), $a_{\rm f}$. The NSs in the initial data of all simulations are spinless.

	Ref.	EOS	C	Q	$a_{\rm i}$	$a_{\rm f}^{\rm NR}$	$a_{\rm f}^{\rm BKL}$	$a_{\rm f,1}$	$a_{\rm f}$
1	[38]	$\Gamma = 2$	0.145	3	−0.5	0.33	0.31	0.31	0.33
2	[38]	$\Gamma = 2$	0.145	3	0.75	0.88	0.85	0.86	0.87
3	[38]	$\Gamma = 2$	0.145	3	0	0.56	0.54	0.53	0.55
4	[38]	$\Gamma = 2$	0.145	5	0	0.42	0.42	0.42	0.42
5	[48]	$\Gamma = 2$	0.145	2	0	0.68	0.61	0.61	0.64
6	[48]	$\Gamma = 2$	0.145	3	0	0.56	0.54	0.53	0.55
7	[48]	$\Gamma = 2$	0.145	4	0	0.48	0.47	0.47	0.47
8	[48]	$\Gamma = 2$	0.145	5	0	0.42	0.42	0.42	0.42
9	[48]	$\Gamma = 2$	0.160	2	0	0.68	0.61	0.62	0.65
10	[48]	$\Gamma = 2$	0.160	3	0	0.55	0.54	0.54	0.55
11	[48]	$\Gamma = 2$	0.178	2	0	0.67	0.61	0.62	0.66
12	[48]	$\Gamma = 2$	0.178	3	0	0.55	0.54	0.54	0.56
13	[43]	$\Gamma = 2$	0.144	3	0	0.56	0.54	0.53	0.54
14	[43]	$\Gamma = 2$	0.144	3	0.5	0.77	0.75	0.75	0.76
15	[43]	$\Gamma = 2$	0.144	3	0.9	0.93	0.90	0.93	0.93
16	[46]	$\Gamma = 2$	0.144	7	0.5	0.67	0.67	0.68	0.68
17	[46]	$\Gamma = 2$	0.144	7	0.7	0.80	0.80	0.81	0.81
18	[46]	$\Gamma = 2$	0.144	7	0.9	0.92	0.91	0.93	0.93
19	[46]	$\Gamma = 2$	0.144	5	0.5	0.71	0.71	0.71	0.71
20	[45]	2H-135	0.131	2	0	0.64	0.61	0.59	0.63
21	[45]	H-135	0.162	2	0	0.67	0.61	0.61	0.66
22	[45]	HB-135	0.172	2	0	0.67	0.61	0.62	0.66
23	[45]	HBs-135	0.172	2	0	0.67	0.61	0.62	0.66
24	[45]	HBss-135	0.174	2	0	0.67	0.61	0.62	0.66
25	[45]	B-135	0.182	2	0	0.67	0.61	0.62	0.67
26	[45]	Bs-135	0.185	2	0	0.66	0.61	0.62	0.67
27	[45]	Bss-135	0.194	2	0	0.65	0.61	0.62	0.67
28	[45]	2H-135	0.131	3	0	0.52	0.54	0.51	0.52
29	[45]	H-135	0.162	3	0	0.56	0.54	0.54	0.56
30	[45]	HB-135	0.172	3	0	0.56	0.54	0.54	0.56
31	[45]	B-135	0.182	3	0	0.55	0.54	0.54	0.56
32	[45]	2H-12	0.118	2	0	0.62	0.61	0.58	0.62
33	[45]	H-12	0.145	2	0	0.66	0.61	0.60	0.64
34	[45]	HB-12	0.153	2	0	0.66	0.61	0.61	0.65
35	[45]	B-12	0.161	2	0	0.67	0.61	0.61	0.66
36	[45]	HB-12	0.153	3	0	0.55	0.54	0.54	0.55
37	[45]	B-12	0.161	3	0	0.56	0.54	0.54	0.56

one of [41,44]: the first half of the label indicates the stiffness of the EOS, with 2H being the stiffest, whereas the second half refers to the NS Arnowitt-Deser-Misner mass at isolation (e.g. 135 stands for $1.35M_\odot$). In this first round of tests, we used the values of $M_{\rm b,torus}$ found with the numerical-relativity simulations and reported in the papers.

TABLE II. Same as Table I.

	Ref.	EOS	C	Q	$a_{\rm i}$	$a_{\rm f}^{\rm NR}$	$a_{\rm f}^{\rm BKL}$	$a_{\rm f,1}$	$a_{\rm f}$
38	[44]	2H-135	0.131	2	0.75	0.87	0.84	0.86	0.89
39	[44]	1.5H-135	0.146	2	0.75	0.89	0.84	0.86	0.89
40	[44]	H-135	0.162	2	0.75	0.91	0.84	0.86	0.90
41	[44]	HB-135	0.172	2	0.75	0.91	0.84	0.86	0.90
42	[44]	B-135	0.182	2	0.75	0.91	0.84	0.86	0.90
43	[44]	2H-135	0.131	2	0.5	0.81	0.77	0.77	0.80
44	[44]	1.5H-135	0.146	2	0.5	0.82	0.77	0.77	0.81
45	[44]	H-135	0.162	2	0.5	0.82	0.77	0.78	0.82
46	[44]	HB-135	0.172	2	0.5	0.83	0.77	0.78	0.82
47	[44]	B-135	0.182	2	0.5	0.83	0.77	0.78	0.82
48	[44]	2H-135	0.131	2	−0.5	0.48	0.44	0.42	0.46
49	[44]	H-135	0.162	2	−0.5	0.51	0.44	0.45	0.50
50	[44]	HB-135	0.172	2	−0.5	0.50	0.44	0.45	0.50
51	[44]	B-135	0.182	2	−0.5	0.49	0.44	0.45	0.51
52	[44]	2H-135	0.131	3	0.75	0.86	0.85	0.86	0.87
53	[44]	1.5H-135	0.146	3	0.75	0.86	0.85	0.86	0.87
54	[44]	H-135	0.162	3	0.75	0.85	0.85	0.86	0.87
55	[44]	HB-135	0.172	3	0.75	0.87	0.85	0.86	0.88
56	[44]	B-135	0.182	3	0.75	0.86	0.85	0.87	0.88
57	[44]	2H-135	0.131	3	0.5	0.74	0.75	0.74	0.75
58	[44]	1.5H-135	0.146	3	0.5	0.75	0.75	0.75	0.76
59	[44]	H-135	0.162	3	0.5	0.76	0.75	0.75	0.77
60	[44]	HB-135	0.172	3	0.5	0.77	0.75	0.76	0.77
61	[44]	B-135	0.182	3	0.5	0.77	0.75	0.76	0.78
62	[44]	HB-135	0.172	3	−0.5	0.32	0.31	0.31	0.34
63	[44]	2H-135	0.131	4	0.75	0.84	0.84	0.85	0.85
64	[44]	H-135	0.162	4	0.75	0.84	0.84	0.86	0.86
65	[44]	HB-135	0.172	4	0.75	0.85	0.84	0.86	0.86
66	[44]	B-135	0.182	4	0.75	0.85	0.84	0.86	0.86
67	[44]	2H-135	0.131	4	0.5	0.70	0.73	0.71	0.71
68	[44]	H-135	0.162	4	0.5	0.73	0.73	0.73	0.73
69	[44]	HB-135	0.172	4	0.5	0.74	0.73	0.74	0.74
70	[44]	B-135	0.182	4	0.5	0.74	0.73	0.74	0.74
71	[44]	2H-135	0.131	5	0.75	0.82	0.84	0.84	0.84
72	[44]	H-135	0.162	5	0.75	0.84	0.84	0.85	0.85
73	[44]	HB-135	0.172	5	0.75	0.84	0.84	0.85	0.85
74	[44]	B-135	0.182	5	0.75	0.85	0.84	0.86	0.86

To make the whole model numerical relativity independent and quick to use, we shall later adopt the method recently reported in [57] for determining $M_{\rm b,torus}$, and we will show that this does not spoil the agreement between the predictions of our model and the numerical-relativity data. It is evident that the difference between $a_{\rm f,1}$ and $a_{\rm f}^{\rm NR}$ increases as the mass ratio Q of the system decreases, or, equivalently, as the symmetric mass ratio ν increases. Given that the final spin parameter results obtained with numerical-relativity simulations have an absolute error $\Delta a_{\rm f}^{\rm NR}$ of 0.01 [39] and that the error of the BKL approach was evaluated to be $\lesssim 0.02$ in [83], we conclude that the method established by Eq. (8) works well for BH-NS systems with symmetric mass ratios up to $\nu = 0.16$, i.e. for $Q \geq 4$,

whereas it almost systematically reaches or exceeds the 0.03 threshold of marginal agreement when $Q \leq 3$. We must, thus, improve Eq. (8) to handle BH-NS systems with $\nu > 0.16$.

As ν increases, the method fails for two reasons. First, the fifth assumption in Sec. II breaks down as $\nu \to 0.25$ (or $Q \to 1$). This is intrinsic to the BKL method which inspired Eq. (8). Second, and generally speaking, in systems with such low mass BHs the tidal fields tend to tear apart the NS completely, as opposed to binaries with higher mass BHs, in which the outer layers of the NS are mainly stripped off. In the former scenario, the binding energy of the star is liberated and the NS matter accretes onto the BH as a collection of particles with total rest mass $M_{\rm b,NS} - M_{\rm b,torus}$, where $M_{\rm b,NS}$ is the total rest mass of the NS, whereas in the latter scenario the NS core plunges into the BH without undergoing complete tidal disruption. We will make the simplifying assumption that in systems with $\nu = 2/9$ ($Q = 2$), the NS undergoes complete tidal disruption, while it does not in systems with $\nu \leq 0.16$ ($Q \geq 4$). When complete tidal disruption is achieved, the NS should not be treated as a body with mass $M_{\rm NS}$, but as a set of particles with total rest mass $M_{\rm b,NS}$, a subset of which accretes onto the BH and has total mass $M_{\rm b,NS} - M_{\rm b,torus}$. We thus propose to describe $Q = 2$ systems, in which tidal disruption is pivotal, with

$$a_{\rm f} = \frac{a_{\rm i} M_{\rm BH}^2 + l_z(\bar{r}_{\rm ISCO,f}, a_{\rm f}) M_{\rm BH}(M_{\rm b,NS} - M_{\rm b,torus})}{[M\{1 - [1 - e(\bar{r}_{\rm ISCO,i}, a_{\rm i})]\nu\} - e(\bar{r}_{\rm ISCO,f}, a_{\rm f}) M_{\rm b,torus}]^2}, \tag{10}$$

instead of with Eq. (8), and to combine the two descriptions by writing

$$a_{\rm f} = \frac{a_{\rm i} M_{\rm BH}^2 + l_z(\bar{r}_{\rm ISCO,f}, a_{\rm f}) M_{\rm BH}\{[1 - f(\nu)]M_{\rm NS} + f(\nu) M_{\rm b,NS} - M_{\rm b,torus}\}}{[M\{1 - [1 - e(\bar{r}_{\rm ISCO,i}, a_{\rm i})]\nu\} - e(\bar{r}_{\rm ISCO,f}, a_{\rm f}) M_{\rm b,torus}]^2}, \tag{11}$$

where $f(\nu)$ governs the transition between the two regimes of Eqs. (8) and (10). This function is currently poorly constrained, given that state-of-the-art BH-NS simulations with $2 < Q < 4$ are available in the literature only for $Q = 3$. To fix $f(\nu)$, we must impose that $f(\nu \geq 2/9) = 1$ and that $f(\nu \leq 0.16) = 0$. Additionally, it is physically reasonable to require the function to be monotonic and therefore that

$$\frac{df}{d\nu} \geq 0 \qquad 0 \leq \nu \leq 0.25.$$

We shall also require it to be C^∞ and to be as simple as possible. These elements do not determine $f(\nu)$ uniquely, of course. All in all, we set

$$f(\nu) = \begin{cases} 0 & \nu \leq 0.16 \\ \frac{1}{2}\left[1 - \cos\left(\frac{\pi(\nu - 0.16)}{2/9 - 0.16}\right)\right] & 0.16 < \nu < 2/9 \\ 1 & 2/9 \leq \nu \leq 0.25 \end{cases} \tag{12}$$

in a Hann window–inspired fashion. Notice that, in the limit of large BH masses, a BH-NS system behaves as a BH binary system with the same physical parameters, so that in Eq. (8) the NS gravitational mass $M_{\rm NS}$ cannot be simply dropped in favor of its baryonic mass $M_{\rm b,NS}$. Moreover, from a merely quantitative point of view, a model with this oversimplification performs worse when tested against numerical-relativity results.

We now compare the predictions of Eqs. (11) and (12) to the results obtained within full general relativity. As anticipated, this is done in the last column of Tables I and II. It is evident that this strategy improves considerably the outcome of Eq. (8) for systems with $Q = 2$ and $Q = 3$ and that, overall, it improves the estimates obtained by simply applying the BKL method to mixed binary mergers.

Figure 1 shows the absolute value of the difference $a_{\rm f} - a_{\rm f}^{\rm NR}$ versus the dummy index running over the 74 rows of Tables I and II. The graph shows that $\max|a_{\rm f} - a_{\rm f}^{\rm NR}| = 0.04$ and that this value is reached only in one case out of 74 total ones. This corresponds to the $\{C = 0.145, Q = 2, a_{\rm i} = 0\}$ simulation of [39,48]. An absolute error $|a_{\rm f} - a_{\rm f}^{\rm NR}| = 0.03$ is instead obtained for the test case $\{C = 0.160, Q = 2, a_{\rm i} = 0\}$ of [39,48]. We notice that both problematic cases have $Q = 2$ and this may be a sign that our model breaks down for low BH masses.

In Fig. 2, we show the distribution of the difference $a_{\rm f} - a_{\rm f}^{\rm NR}$ that follows from the results reported in Tables I and II. As is evident, the errors are concentrated in the interval $-0.01 \leq a_{\rm f} - a_{\rm f}^{\rm NR} \leq 0.01$, where 61 of the 74 tests fall. Moreover, about a quarter of the final spin values are reproduced exactly. The sum of all the differences $a_{\rm f} - a_{\rm f}^{\rm NR}$

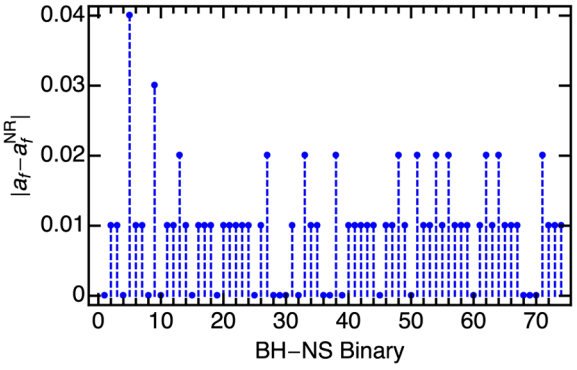

FIG. 1 (color online). $|a_{\rm f} - a_{\rm f}^{\rm NR}|$ is shown for all entries in Tables I and II. The horizontal axis is the dummy that runs through both tables.

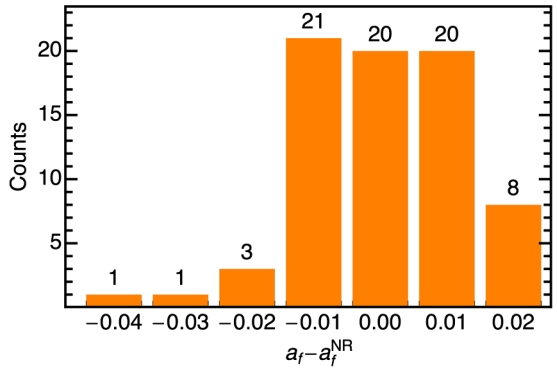

FIG. 2 (color online). $a_f - a_f^{NR}$ distribution for all entries in Tables I and II.

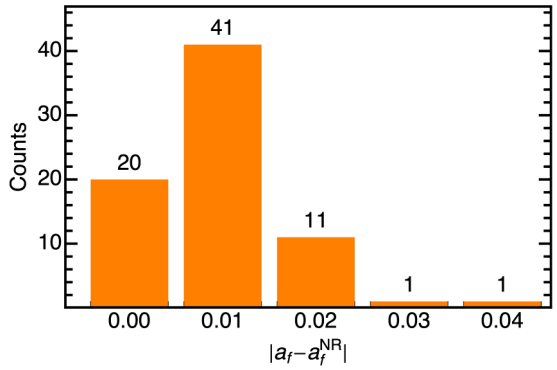

FIG. 3 (color online). $|a_f - a_f^{NR}|$ distribution for all entries in Tables I and II.

yields 0.02, so that $\sum_{n=1}^{74}(a_f - a_f^{NR})_n/74 = 0.00$.[4] In Fig. 3, we consider the distribution of the absolute difference $|a_f - a_f^{NR}|$ and show that it rapidly drops after 0.02. Given that the error on the a_f^{NR}'s is $\Delta a_f^{NR} = 0.01$, 61 numerical-relativity results out of 74, i.e. more than 80% of the cases, are reproduced within the numerical-relativity error.

To determine the absolute error on our predictions, we begin by observing that (1) our model is built against numerical-relativity data with an absolute error $\Delta a_f^{NR} = 0.01$; (2) it is based on the BKL approach, for which the average error found in [83] is ~ 0.02; and (3) the average error yielded by our comparisons against numerical-relativity data is $\langle |a_f - a_f^{NR}| \rangle = \sum_{n=1}^{74} |a_f - a_f^{NR}|_n/74 = 0.01$. Further, the same average error is obtained if the average $\langle |a_f - a_f^{NR}| \rangle$ is marginalized to a given mass ratio Q or initial BH spin parameter value a_i, among the ones available in Tables I and II. This is shown in the second column of Table III. Additionally, the fourth column of the same table shows that the marginalized averages $\langle a_f - a_f^{NR} \rangle$ are such that their absolute value is 0.01 at the most. All in all, if we take an error $\Delta a_f = 0.01$ on our predictions, these are found to be compatible with the numerical-relativity results in 72 test cases out of 74, i.e. about 97%.

[4]This rounding up is justified by the fact that numerical-relativity results for the final spin parameter have an error $\Delta a_f^{NR} \sim 0.01$.

TABLE III. Average $|a_f - a_f^{NR}|$ and $a_f - a_f^{NR}$ for a given physical parameter, indicated in the first column. The second and fourth columns refer to predictions for a_f obtained by substituting for $M_{b,torus}$ in Eq. (11) the results found in the numerical-relativity simulations reported in [38,41,43,45,46,48], whereas the third and fifth columns refer to predictions for a_f obtained by using the model described in [57] to calculate the $M_{b,torus}$'s.

Fix parameter	$\langle \lvert a_f - a_f^{NR} \rvert \rangle$		$\langle a_f - a_f^{NR} \rangle$	
$Q = 2$	0.01	0.01	−0.01	−0.01
$Q = 3$	0.01	0.01	0.00	0.01
$Q = 4$	0.01	0.01	0.01	0.01
$Q = 5$	0.01	0.01	0.01	0.01
$Q = 7$	0.01	0.01	0.01	0.01
$a_i = -0.5$	0.01	0.01	0.00	0.00
$a_i = 0$	0.01	0.01	−0.01	−0.01
$a_i = 0.5$	0.01	0.01	0.00	0.00
$a_i = 0.7$	0.01	0.01	0.01	0.01
$a_i = 0.75$	0.01	0.01	0.01	0.01
$a_i = 0.9$	0.01	0.01	0.01	0.01

So far, when comparing the predictions of Eqs. (11) and (12) to the BH-NS merger results available in the literature, we exploited the numerical-relativity prediction for $M_{b,torus}$. This allowed us to test and validate Eqs. (11) and (12) and to determine the average error $\Delta a_f^{NR} \simeq 0.01$. If we wish to apply such a method to a large number and variety of BH-NS binaries, we must consider another way of obtaining $M_{b,torus}$. As mentioned previously, we choose to use the simple two-parameter model, fitted to existing numerical results, recently reported by Foucart in [57]. This provides an estimate for $M_{b,torus}$, given a binary mass ratio, an initial BH spin parameter, and a NS compactness. In Fig. 4 we show the absolute values of the difference $a_f - a_f^{NR}$ obtained when using the approach of [57] to calculate $M_{b,torus}$; this figure must be compared to Fig. 1. We find that the two problematic test cases, i.e. ones with $|a_f - a_f^{NR}| > 0.02$, are the same ones encountered previously, that is, cases 5 and 9,

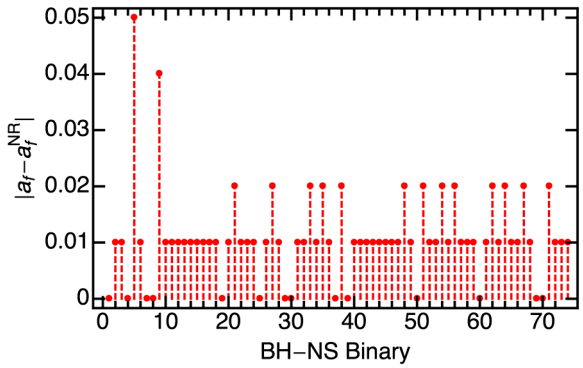

FIG. 4 (color online). Same as Fig. 1, but using the predictions of [57] for $M_{b,torus}$ in Eq. (11).

and that this time they yield $|a_f - a_f^{NR}|$ equal to 0.05 and 0.04, respectively.

As far as the distribution of the differences $a_f - a_f^{NR}$ is concerned, the sum over all differences $a_f - a_f^{NR}$ yields 0.04 (as opposed to 0.02). The averages $\sum_{n=1}^{74}(a_f - a_f^{NR})_n/74$ and $\sum_{n=1}^{74}|a_f - a_f^{NR}|_n/74$ are 0.00 and 0.01, respectively. The averages $\langle|a_f - a_f^{NR}|\rangle$ and $\langle a_f - a_f^{NR}\rangle$ marginalized to a given binary mass ratio or an initial BH spin parameter are reported in the third and fifth columns of Table III, respectively. Their behavior does not vary significantly from the analysis reported previously. The $|a_f - a_f^{NR}|$ distribution obtained combining Eqs. (11) and (12) with the model of [57] is shown in Fig. 5 and should be compared to the one in Fig. 3. The distribution is once again peaked at 0.01, and it falls off above 0.02. Recalling that $\Delta a_f^{NR} = 0.01$, an agreement within the numerical-relativity error is found in 59 (as opposed to 61) cases out of 74. If, moreover, we take an error $\Delta a_f = 0.01$ on our predictions, we observe once again that 72 of them out of 74 are compatible with the numerical-relativity results.

In conclusion, the tests and analyses performed show that the model formulated in Eqs. (11) and (12) is robust. Using our tests against numerical-relativity results, we argued that $\Delta a_f = 0.01$. A more conservative statement is that the error on our prediction for the final spin parameter a_f is $\Delta a_f \lesssim 0.02$. This allows us to include in Δa_f the error $\Delta a_f^{NR} = 0.01$ on numerical-relativity results against which our model is built. We note that $\Delta a_f \lesssim 0.02$ is compatible with $\sim 1\%$ variations of the term $a_i M_{BH}^2$ appearing in Eq. (11). If we interpret this $\sim 1\%$ variation as a representation of possible "glitches" in the transition from the quasiequilibrium initial data to the dynamical evolution of the Einstein equations in a numerical simulation, we see that we are indeed "inheriting" a ~ 0.01 contribution to Δa_f in building our model against numerical-relativity results and that this contribution is at least comparable to the ones introduced by all other approximations behind Eqs. (11) and (12). Further, we stress once more that

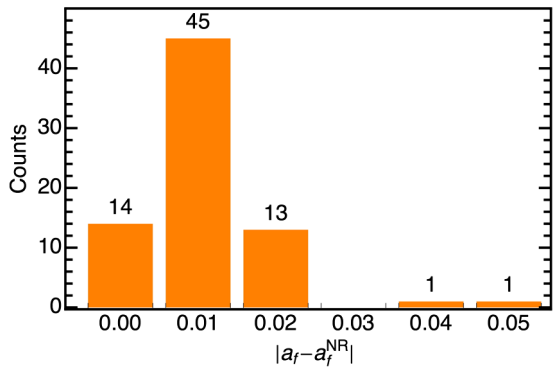

FIG. 5 (color online). $|a_f - a_f^{NR}|$ distribution obtained when using the predictions of [57] for $M_{b,torus}$ in Eq. (11).

$\Delta a_f \lesssim 0.02$ is compatible with the average error, found in [83], for the BKL model, which inspired this work. All these conclusions remain valid even when combining Eqs. (11) and (12) with the method of [57] to calculate $M_{b,torus}$.

It is striking that our simple model to determine a_f paired with [57] obtains such an excellent agreement with the fully general-relativistic numerical simulations of BH-NS mergers. One must always bear in mind, however, that there still are large, unexplored portions of the parameter space and that this prevents us from thoroughly testing our approach to determine a_f.

A. Testing the final mass predictions

So far, we tested only one of the two predictions that our model enables us to make. In this section we separately test the predictions for the mass M_f of the BH remnant, stemming from Eq. (9). According to the "no-hair" theorem of general relativity, the final spin parameter and mass of an electrically neutral BH are the only two quantities characterizing the BH itself. A model capable of accurately predicting both a_f and M_f would therefore fully describe the BH remnant.

The numerical simulations of BH-NS mergers performed by the Kyoto-Tokyo group reported in [44,45,48] allow us to test the outcome of Eq. (9) and to establish the error associated with it. In Tables IV and V, we collect the numerical-relativity data for the mass of the BH remnant and compare it to our predictions. The first six columns of the tables follow Tables I and II, including the numbering of the simulations appearing in column one. The seventh and eighth columns provide the relative error on the remnant masses obtained when comparing the predictions of Eq. (9) to the numerical-relativity results. Following [44,45,48], two forms of the remnant mass are considered: the gravitational mass M_f, and the irreducible mass

$$M_{irr,f} = M_f\sqrt{\frac{1+\sqrt{1-a_f^2}}{2}}. \tag{13}$$

Both M_f and $M_{irr,f}$ are divided by the sum M of the initial gravitational masses M_{BH} and M_{NS}. In the remaining columns of the table, we give the relative error on the $l = 2$, $m = 2$, $n = 0$ quasinormal mode (QNM) frequency f_{220}^{QNM}, and damping time τ_{220}^{QNM} of the BH remnant [88]. Both a_f and M_f must be used to calculate f_{220}^{QNM} and τ_{220}^{QNM}, so that $\epsilon(f_{220}^{QNM})$ and $\epsilon(\tau_{220}^{QNM})$ give us a sense of how our errors on the final BH spin parameter and mass propagate. The terms of comparison for the QNM frequencies and damping times are obtained by using the final mass and spin parameter values given in [44,45,48] and plugging them in the formulas of [88].

A maximum relative error of 1% and 2% is found for $\bar{M}_f = M_f/M$ and $\bar{M}_{irr,f} = M_{irr,f}/M$, respectively, with the

TABLE IV. Tests against numerical-relativity results. The first six columns are organized as in Tables I and II. The last four columns show the relative error on the BH remnant gravitational mass in units of the system initial mass, $\bar{M}_{\rm f}$, on its irreducible mass in units of the system initial mass, $\bar{M}_{\rm irr,f}$, and on its $l=2$, $m=2$, $n=0$ quasinormal mode frequency, $f_{220}^{\rm QNM}$, and damping time, $\tau_{220}^{\rm QNM}$.

	Ref.	EOS	C	Q	$a_{\rm i}$	$\epsilon(\bar{M}_{\rm f})$	$\epsilon(\bar{M}_{\rm irr,f})$	$\epsilon(f_{220}^{\rm QNM})$	$\epsilon(\tau_{220}^{\rm QNM})$
5	[48]	$\Gamma=2$	0.145	2	0	0.00	0.01	0.03	0.02
6	[48]	$\Gamma=2$	0.145	3	0	0.00	0.00	0.01	0.00
7	[48]	$\Gamma=2$	0.145	4	0	0.00	0.00	0.00	0.00
8	[48]	$\Gamma=2$	0.145	5	0	0.00	0.00	0.01	0.00
9	[48]	$\Gamma=2$	0.160	2	0	0.00	0.01	0.02	0.01
10	[48]	$\Gamma=2$	0.160	3	0	0.00	0.00	0.01	0.00
11	[48]	$\Gamma=2$	0.178	2	0	0.00	0.01	0.01	0.00
12	[48]	$\Gamma=2$	0.178	3	0	0.01	0.00	0.00	0.01
20	[45]	2H-135	0.131	2	0	0.00	0.00	0.01	0.00
21	[45]	H-135	0.162	2	0	0.00	0.00	0.01	0.00
22	[45]	HB-135	0.172	2	0	0.00	0.01	0.01	0.00
23	[45]	HBs-135	0.172	2	0	0.00	0.01	0.01	0.00
24	[45]	HBss-135	0.174	2	0	0.00	0.01	0.01	0.00
25	[45]	B-135	0.182	2	0	0.01	0.00	0.01	0.01
26	[45]	Bs-135	0.185	2	0	0.01	0.00	0.00	0.01
27	[45]	Bss-135	0.194	2	0	0.01	0.00	0.00	0.02
28	[45]	2H-135	0.131	3	0	0.00	0.00	0.00	0.00
29	[45]	H-135	0.162	3	0	0.01	0.00	0.01	0.01
30	[45]	HB-135	0.172	3	0	0.01	0.00	0.01	0.01
31	[45]	B-135	0.182	3	0	0.01	0.01	0.00	0.01
32	[45]	2H-12	0.118	2	0	0.00	0.00	0.00	0.00
33	[45]	H-12	0.145	2	0	0.00	0.00	0.01	0.01
34	[45]	HB-12	0.153	2	0	0.00	0.00	0.01	0.00
35	[45]	B-12	0.161	2	0	0.00	0.00	0.01	0.00
36	[45]	HB-12	0.153	3	0	0.00	0.00	0.00	0.00
37	[45]	B-12	0.161	3	0	0.01	0.01	0.01	0.01

2% occurring only once. The errors on $f_{220}^{\rm QNM}$ and $\tau_{220}^{\rm QNM}$, on the other hand, are at the most 4% and 5%, respectively. It is noteworthy that the second contribution in Eq. (9), i.e. the energy loss due to GW emission, is crucial in obtaining such accurate results: if we do not include it, the maximum error on $f_{220}^{\rm QNM}$, for example, is 9%.

If we use input from the model of [57] and repeat these tests on $\bar{M}_{\rm f}$, $\bar{M}_{\rm irr,f}$, $f_{220}^{\rm QNM}$, and $\tau_{220}^{\rm QNM}$, the maximum errors we obtain are 2%, 3%, 5%, and 4%, respectively. The panels of Fig. 6 show the distributions of the relative errors $\epsilon(\bar{M}_{\rm f})$, $\epsilon(\bar{M}_{\rm irr,f})$, $\epsilon(f_{220}^{\rm QNM})$, and $\epsilon(\tau_{220}^{\rm QNM})$ obtained when using Eqs. (9), (11), and (12) in combination with [57]. As for the tests performed with the numerical-relativity values of $M_{\rm b,torus}$, these distributions are peaked around ~0.00–0.01, and errors higher than 2% are rare. We stress once more that large portions of the parameter space of BH-NS binaries are currently unexplored, thus preventing us from testing our approach thoroughly.

TABLE V. Same as Table IV.

	Ref.	EOS	C	Q	$a_{\rm i}$	$\epsilon(\bar{M}_{\rm f})$	$\epsilon(\bar{M}_{\rm irr,f})$	$\epsilon(f_{220}^{\rm QNM})$	$\epsilon(\tau_{220}^{\rm QNM})$
38	[44]	2H-135	0.131	2	0.75	0.01	0.02	0.04	0.04
39	[44]	1.5H-135	0.146	2	0.75	0.00	0.01	0.00	0.00
40	[44]	H-135	0.162	2	0.75	0.00	0.00	0.02	0.03
41	[44]	HB-135	0.172	2	0.75	0.00	0.01	0.02	0.03
42	[44]	B-135	0.182	2	0.75	0.00	0.01	0.02	0.03
43	[44]	2H-135	0.131	2	0.5	0.00	0.00	0.01	0.01
44	[44]	1.5H-135	0.146	2	0.5	0.00	0.00	0.01	0.01
45	[44]	H-135	0.162	2	0.5	0.00	0.00	0.00	0.00
46	[44]	HB-135	0.172	2	0.5	0.00	0.00	0.01	0.01
47	[44]	B-135	0.182	2	0.5	0.00	0.01	0.01	0.01
48	[44]	2H-135	0.131	2	−0.5	0.00	0.00	0.01	0.01
49	[44]	H-135	0.162	2	−0.5	0.00	0.00	0.01	0.00
50	[44]	HB-135	0.172	2	−0.5	0.00	0.00	0.00	0.00
51	[44]	B-135	0.182	2	−0.5	0.00	0.00	0.01	0.01
52	[44]	2H-135	0.131	3	0.75	0.00	0.01	0.02	0.01
53	[44]	1.5H-135	0.146	3	0.75	0.00	0.01	0.01	0.02
54	[44]	H-135	0.162	3	0.75	0.00	0.01	0.02	0.04
55	[44]	HB-135	0.172	3	0.75	0.00	0.00	0.01	0.02
56	[44]	B-135	0.182	3	0.75	0.01	0.00	0.02	0.05
57	[44]	2H-135	0.131	3	0.5	0.00	0.00	0.01	0.01
58	[44]	1.5H-135	0.146	3	0.5	0.00	0.00	0.01	0.01
59	[44]	H-135	0.162	3	0.5	0.00	0.00	0.01	0.01
60	[44]	HB-135	0.172	3	0.5	0.01	0.00	0.01	0.01
61	[44]	B-135	0.182	3	0.5	0.01	0.00	0.00	0.02
62	[44]	HB-135	0.172	3	−0.5	0.00	0.00	0.01	0.00
63	[44]	2H-135	0.131	4	0.75	0.00	0.01	0.01	0.01
64	[44]	H-135	0.162	4	0.75	0.01	0.00	0.02	0.04
65	[44]	HB-135	0.172	4	0.75	0.01	0.00	0.01	0.02
66	[44]	B-135	0.182	4	0.75	0.01	0.01	0.00	0.02
67	[44]	2H-135	0.131	4	0.5	0.00	0.00	0.01	0.01
68	[44]	H-135	0.162	4	0.5	0.01	0.01	0.01	0.01
69	[44]	HB-135	0.172	4	0.5	0.01	0.01	0.01	0.01
70	[44]	B-135	0.182	4	0.5	0.01	0.01	0.01	0.01
71	[44]	2H-135	0.131	5	0.75	0.00	0.01	0.02	0.03
72	[44]	H-135	0.162	5	0.75	0.01	0.00	0.01	0.02
73	[44]	HB-135	0.172	5	0.75	0.01	0.00	0.00	0.02
74	[44]	B-135	0.182	5	0.75	0.01	0.00	0.00	0.03

IV. RESULTS

We now review the main results obtained by systematically exploring the space of parameters of BH-NS systems using the model described so far. More specifically, we vary

(i) the initial spin parameter of the BH, $a_{\rm i}$, reaching a maximum value of 0.99;
(ii) the binary mass ratio, Q, between 2 and 10;
(iii) the NS mass, between $1.2M_{\odot}$ and $2.0M_{\odot}$, compatibly with the measurement reported in [89];
(iv) the NS compactness. In particular, we use the WFF1 EOS [90] and the PS EOS [91] as representatives of the softest and stiffest possible EOS, yielding the most and least compact NSs, respectively. Thus, for a given NS mass we consider the compactness of a NS governed by the WFF1 EOS and the one of a NS described by the PS EOS. We also quote results for the APR2 EOS [92] since this is the most complete nuclear many-body study to date.

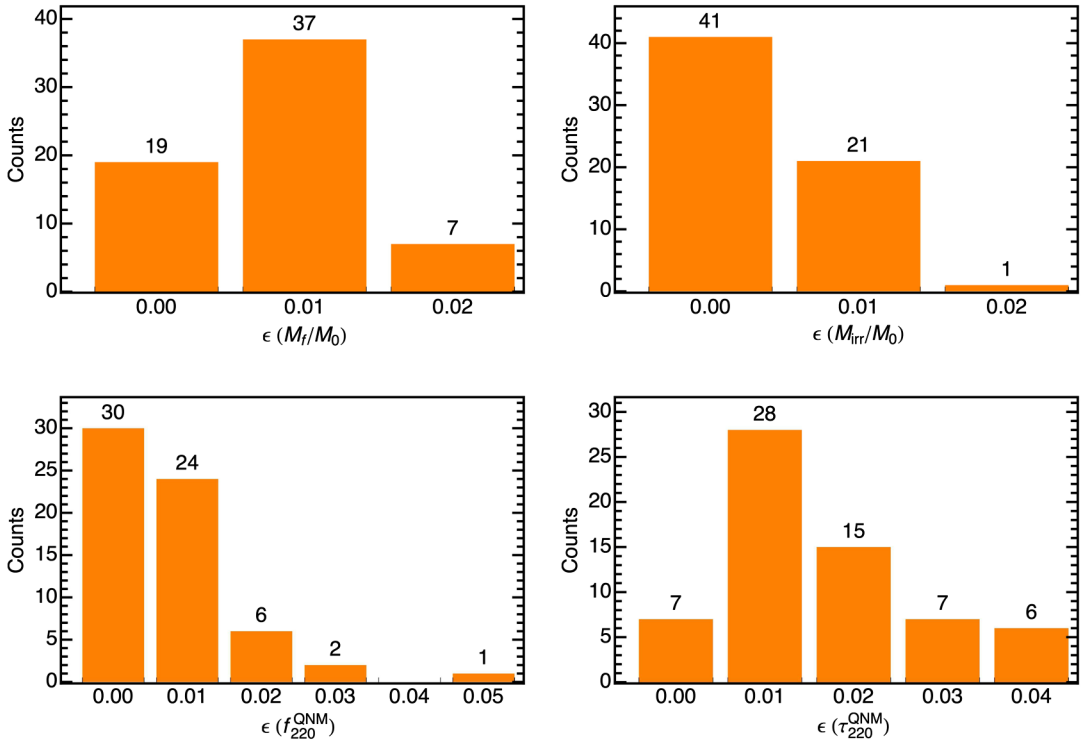

FIG. 6 (color online). Distribution of the relative errors $\epsilon(M_f/M)$, $\epsilon(M_{irr,f}/M)$, $\epsilon(f_{220}^{QNM})$, and $\epsilon(\tau_{220}^{QNM})$ obtained from Eqs. (9), (11), and (12) in combination with [57] for test cases in Tables IV and V for which information on the BH remnant mass is provided in the references.

The choices regarding the EOS are discussed in detail in the Appendix.

We analyze the behavior of a_f in the relevant space of parameters, examining its maximum possible value; we further compare the outcome of BH-NS mergers and BH-BH mergers in terms of the $l = m = 2, n = 0$ quasinormal mode frequency and show that the comparison is EOS dependent. When comparing to binary black holes, we apply the fitting formula of [83] to determine the final spin parameter of the their remnants, and we neglect the last term in Eq. (9) to estimate the mass of their remnants.[5] More accurate predictions for M_f are possible for BH-BH binaries, e.g. [85]; if we were to rely on them, however, we would be comparing predictions with a different degree of accuracy, thus mixing the *physical* consequences of replacing the lower mass BH of a binary BH with a NS to effects due to the different precision underlying the predictions under comparison.

A. Maximum final spin parameter

An important aspect to investigate when studying the final spin of the BH remnant of compact binary mergers is its maximum value. According to the cosmic censorship conjecture, the spin parameter of a BH cannot exceed unity [94]. Indirect support to the conjecture was provided by the recent numerical-relativity simulations of BH-NS mergers [44]. The extrapolation of the results of the numerical simulations to the case of an extremely spinning BH with $a_i = 1$ (merging with an irrotational NS) yielded $a_f \sim 0.98$. It was suggested that simulations with mass ratio higher than $Q = 4$ and (nearly) extremal initial BH spin should be performed in order to assess whether $a_f \lesssim 0.98 (< 1)$ is a universal bound for BH-NS binary mergers or not.

Our model does not predict the formation of overspinning ($a_f > 1$) BHs for BH-NS binaries with an extremal initial BH spin and any symmetric mass ratio. We notice that, all else being fixed, the softer the EOS, the higher the final spin parameter a_f. We thus suggest performing fully general-relativistic numerical simulations of systems with (nearly) extremal initial BH spin parameter and a soft NS EOS to assess the bound on $a_f < 1$ for BH-NS binary mergers.

To determine the maximum final spin parameter, we consider our data and *extrapolate* it to $a_i = 1$. We perform the extrapolations on two different sets of data: in one case we use all our data, i.e. with a_i up to 0.99, whereas in the other we consider only $a_i \leq 0.9$. This allows us to cross-check our predictions obtained within the untested region of the parameter space $0.9 < a_i \leq 1$, thus making our conclusions more robust. The highest final spin parameters we obtain are for $Q = 10$, or $\nu \simeq 0.083$. The WFF1, PS, and APR2 EOS all yield a maximum final spin parameter $a_f = 1.00$, compatible with the $a_f \sim 0.98$ bound pinpointed in [44]. Even though we previously determined

[5]This is how the BH remnant properties are determined in [93].

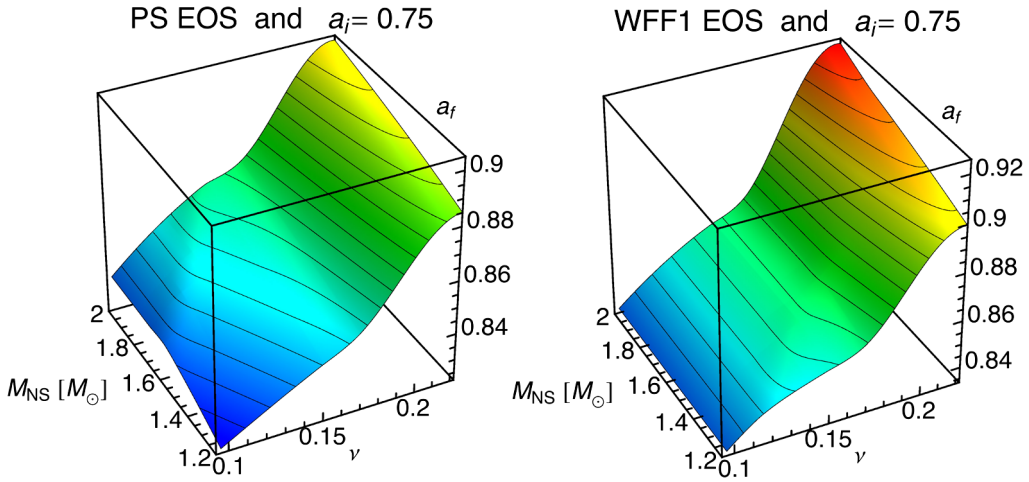

FIG. 7 (color online). The final spin parameter of BH-NS systems is shown as a function of the NS mass and the symmetric mass ratio; the initial spin parameter of the BH is set to 0.75. Results in the left/right panel refer to the PS/WFF1 EOS.

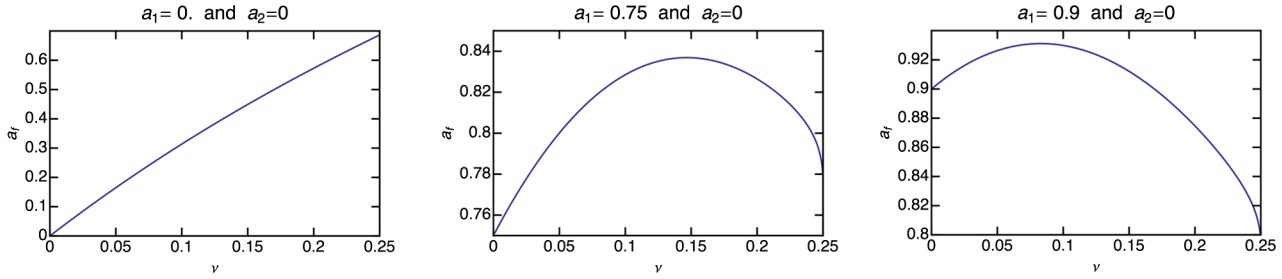

FIG. 8 (color online). Final spin parameter for binaries with a primary spinning BH and a secondary nonspinning BH. From left to right, the initial spin parameter of the spinning BH is set to 0, 0.75, and 0.9. The curves were obtained with the fitting formula of [83].

that our predictions have an error $\Delta a_f \lesssim 0.02$ (see discussion in Sec. III), we believe it is worth mentioning that we find $\max a_f = 0.997$, an "empirical" result that is very close to Thorne's limit of 0.998 [95].

B. Dependence of the BH remnant on the NS EOS

The main feature that appears when comparing results for different EOSs is that final spin parameter of the BH remnant, a_f, can depend on the EOS of the NS in the mixed binary progenitor (all else being fixed). This happens because different EOSs yield different torus masses. An example of this EOS dependence is provided in Fig. 7, where binaries with $a_i = 0.75$ and two possible EOSs, the WFF1 and the PS, are considered. The EOS dependence of a_f may be better understood by carefully examining the case of BH-BH binaries. Figure 8 shows that, given a binary with a nonspinning secondary BH and a primary BH with initial spin parameter a_i, there is a specific symmetric mass ratio that yields the maximum a_f: its value varies monotonically from 0.25 to 0 as the a_i runs from 0 to 1. More specifically, the first panel shows that for nonspinning binary BHs, higher values of a_f are favored by high symmetric mass ratios (i.e. it is "easier" to spin up a Schwarzschild BH with a mass comparable to the one of the BH itself), while this is not true in the other two panels, in which the primary BH is rotating. In the case of BH-NS systems, as one varies ν and M_{NS}, the BH mass changes along with the mass accreting onto the BH: in the case of disruptive mergers, the latter depends on the EOS and this explains why the spin of the BH remnant depends on the EOS of the NS in the progenitor for BH-NS disruptive mergers.

Having shown that a_f may depend on the NS EOS and bearing in mind that M_f may too,[6] this means that information about the NS EOS is "coded" in the properties of the BH remnant. This in turn implies that the QNM spectrum of the BH remnant may (1) be affected by the EOS and (2) deviate from the BH-BH behavior. In Fig. 9 we compare the BH remnant of BH-NS mergers to the BH remnant of BH-BH mergers. We show the difference between the QNM frequency f_{220}^{QNM} of the BH remnant of

[6]This is more straightforward to comprehend: NSs differing only for the EOS differ in compactness and may thus accrete different amounts of matter in disruptive mergers with a BH, e.g. [44].

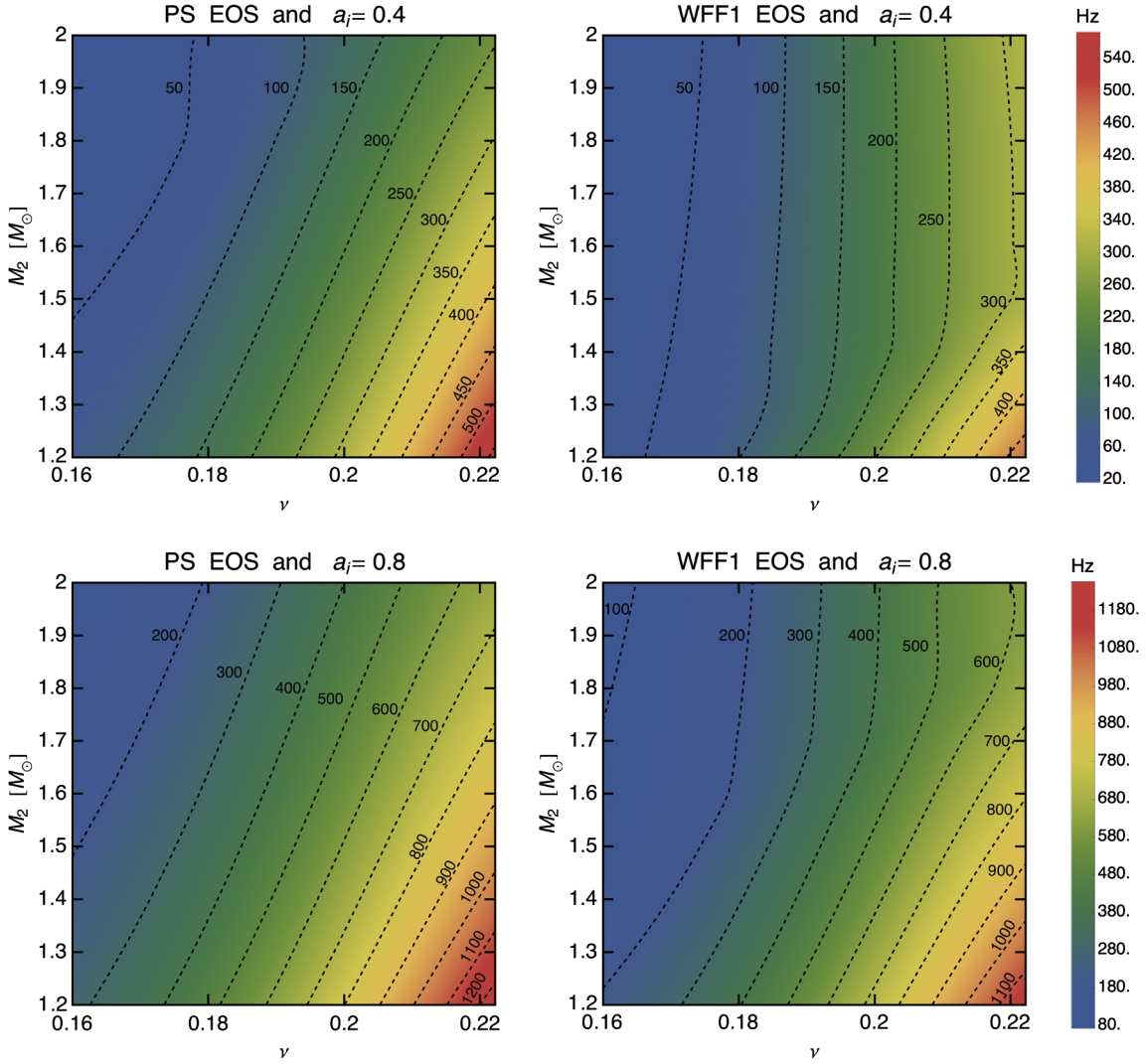

FIG. 9 (color online). Difference, in Hz, between the $l = m = 2$, $n = 0$ quasinormal mode frequency, $f_{220}^{\rm QNM}$, of the BH remnant of a BH-NS merger and of a BH-BH merger with the same secondary mass M_2, symmetric mass ratio ν, and initial spin parameters. The NS and secondary BH initial spin is always set to zero. The primary BH initial spin parameter is 0.4 and 0.8 in the top and bottom panels, respectively.

a BH-NS merger and of a BH-BH merger with the same secondary mass, symmetric mass ratio, and initial spin parameters. The final spin parameter and mass of the binary BHs are determined using the method of [83] and Eq. (9) without the last term, respectively. All QNM frequencies are calculated using the fitting formula of [88].

Our results confirm that the mixed binaries we expect to see the most of, i.e. those with $\nu \sim 0.11$ [3], do indeed behave like binary BHs in terms of GW emission during the ringdown epoch: this is positive for template design and GW detection. In Fig. 9 we show our results in the region above $\nu = 0.16$ for binaries with $a_{\rm i} = 0.4$ and $a_{\rm i} = 0.8$, and we contrast the PS EOS with the WFF1 EOS. We find that for $\nu \sim 0.16$ (or $Q \sim 4$) the BH remnant QNM frequency $f_{220}^{\rm QNM}$ deviates from its BH-BH binary value by $\lesssim 100$ Hz for both soft and stiff EOSs, unless the initial BH spin parameter is particularly high and the NS EOS is very stiff (bottom, left panel of Fig. 9). The NS thus leaves a (small) "trace" in the QNM frequency: for binaries with a BH with moderate to high spin and a symmetric mass ratio $\nu \lesssim 0.16$, one could in principle determine whether the source of a detected GW coalescence signal was a BH-BH or a BH-NS binary by separately analyzing the inspiral and the ringdown epochs. The former epoch would be identical for a mixed binary and a BH binary with the same physical parameters, because tidal deformations of the NS in a mixed binary with $\nu \lesssim 0.16$ are not expected to significantly alter the inspiral epoch of the GW signal [15]. Looking at the ringdown epoch would therefore complement the idea of pinning down the presence of the NS from the inspiral. Constraining the NS EOS in the region of the parameter space around $\nu \sim 0.16$ by measuring $f_{220}^{\rm QNM}$ appears, instead, to be difficult.

For systems with high symmetric mass ratios, on the other hand, the difference in $f_{220}^{\rm QNM}$ may be high, suggesting the interesting prospect of constraining the NS EOS through the measurement of the properties of the BH remnant. If we now focus on the high ν region of the panels in Fig. 9, we see that the deviations in $f_{220}^{\rm QNM}$ from the BH-BH case are particularly evident for $\nu \gtrsim 0.2$ and a high initial BH spin parameter. This and all other features of the bottom panels in Fig. 9 may be compared to those of the panels in Fig. 7, showing that they are "inherited" from the behavior of $a_{\rm f}$. At high ν's and $a_{\rm i}$'s, the difference between the $f_{220}^{\rm QNM}$ of the BH remnant of a BH-NS merger and the one of a BH-BH merger ranges from ~600 Hz to ~1200 Hz. The NS EOS therefore leaves an imprint on the QNM frequency of the BH remnant, although one should bear in mind that we are comparing two (extreme) EOSs that are on opposite ends in terms of stiffness, and this makes the differences between the left and the right panels of Fig. 9 particularly prominent. A comparison between results for the WFF1 EOS and the APR2 EOS, which yield NSs relatively similar in terms of compactness (see Fig. 11), tells us that in order to be able to properly discriminate between similar candidate nuclear EOSs, one would need to be able to perform measurements of $f_{220}^{\rm QNM}$ with a precision the order of ~10 Hz.

Being able to perform measurements of $f_{220}^{\rm QNM}$ for the BH remnant of BH-NS mergers requires that the QNM itself is excited during the coalescence. If this happens, $f_{220}^{\rm QNM}$ influences the value of the cutoff frequency $f_{\rm cut}$ of the GW spectrum of the mixed binary coalescence.[7] The extrapolation of the results of the numerical-relativity simulations reported in [44] shows, in particular, that $f_{\rm cut} \simeq f_{220}^{\rm QNM}$ for $C \gtrsim 0.18$ in mixed binaries with $\nu \simeq 0.139$ (or $Q = 5$) and $a_{\rm i} = 0.75$, or for $C \gtrsim 0.19$ in binaries when $a_{\rm i} = 0$ and $\nu \simeq 0.22$ ($Q = 2$) or $\nu \simeq 0.1875$ ($Q = 3$) and $a_{\rm i} = 0.5$. An increase in $a_{\rm i}$ corresponds to an increase in the lower bound on C that allows for $f_{\rm cut} \simeq f_{220}^{\rm QNM}$ to happen at a given mass ratio; on the other hand, the higher the mass of the BH at a given $a_{\rm i}$ and C, the closer $f_{\rm cut}$ will be to $f_{220}^{\rm QNM}$. The ~0.19 threshold on the NS compactness encountered above corresponds to $M_{\rm NS} \gtrsim 1.33 M_\odot$ for the WFF1 EOS, to $M_{\rm NS} \gtrsim 1.48 M_\odot$ for the APR2 EOS, and to $M_{\rm NS} \gtrsim 1.93 M_\odot$ for the PS EOS. We thus see that there is the virtual possibility of constraining the NS EOS with the measurement of the gravitational radiation emitted by those binaries for which $f_{\rm cut} \simeq f_{220}^{\rm QNM}$. This scenario, as said, concerns NSs with high compactness and would thus provide constraints for *soft* EOSs. We note that the observation of tidal effects in the phase of the gravitational radiation emitted during the inspiral [15,96] and in the cutoff frequency when $f_{\rm cut} < f_{220}^{\rm QNM}$ [13,44] favors placing constraints on stiff EOSs, so that measurements in $f_{\rm cut} \sim f_{220}^{\rm QNM}$ scenarios would be complementary.

[7] See [44] for explanations on what determines $f_{\rm cut}$ and for examples of gravitational waveform spectra.

V. CONCLUSIONS AND REMARKS

In this paper we presented a model for predicting the final spin parameter, $a_{\rm f}$, and mass, $M_{\rm f}$, of the BH remnant of BH-NS coalescing binaries in quasicircular orbits, with initial BH spin of arbitrary magnitude and parallel to the orbital angular momentum, with arbitrary mass ratio, and with arbitrary NS mass and cold, barotropic equation of state. The parameter space just outlined could in principle be investigated entirely with numerical-relativity simulations; in practice, however, the process would be very time and resource consuming, because simulations are still very expensive in terms of computational costs.

Our starting point was the phenomenological model of Buonanno, Kidder, and Lehner for the final spin of binary BH mergers [74], which we modified to account for (1) energy loss via gravitational wave emission during the inspiral and (2) the possible formation of an accretion torus in the case of disruptive mergers. We tested our model by comparing its predictions to the recent numerical-relativity simulation results available in the literature. We were able to achieve good agreement down to a mass ratio of $M_{\rm BH}/M_{\rm NS} = 2$, albeit introducing an additional ingredient in the formulation of the model for $2 < M_{\rm BH}/M_{\rm NS} < 4$, which is currently poorly constrained. We obtained an absolute error on $a_{\rm f}$ of 0.02, which is compatible with the one of the BKL approach [74,83]. For the final gravitational and irreducible (normalized) masses of the BH remnant, $M_{\rm f}$ and $M_{\rm irr,f}$, we found a relative error of 1%. These errors then propagate in the calculation of the $l = m = 2$, $n = 0$ quasinormal mode frequency $f_{220}^{\rm QNM}$ and damping time $\tau_{220}^{\rm QNM}$ of the remnant BH, and they yield maximum relative errors of 4% and 5%, respectively. These relative errors are, however, safely $\leq 2\%$ in the vast majority of test cases. Combining this method with input for the torus remnant mass from the two-parameter model, fitted to existing numerical results, recently reported by Foucart in [57], the error $\Delta a_{\rm f} \simeq 0.02$ is preserved and so is the behavior of the relative errors on $M_{\rm f}$, $M_{\rm irr,f}$, $f_{220}^{\rm QNM}$, and $\tau_{220}^{\rm QNM}$ (see Figs. 4 and 6).

The tests we performed against the available numerical-relativity results were successful, especially considering the limitations of our simple approach. This implies that the outcome of the complicated merger dynamics of BH-NS binaries may be understood in fairly simple terms, at least when the BH initial spin and orbital angular momentum directions are parallel and the inspiral orbit is quasicircular. Equations (9), (11), and (12) presented here along with the fit of Foucart to the torus remnant mass [57] constitute an easy-to-use analytical model that describes the remnant of BH-NS mergers.

Notwithstanding the good performance of the model in the tests, its predictions should be taken with "a grain of salt," as large portions of the parameter space of BH-NS binaries are currently unexplored, hampering a thorough test of our approach.

The approach presented and tested in the first part of this work was then employed to span the space of parameters consisting of the binary (symmetric) mass ratio, the BH initial spin, the NS mass, and the NS equation of state. This enabled us to gain a sense of the behavior of the properties of the BH remnant in this fourfold space of parameters and to pinpoint some interesting aspects which, we believe, deserve being verified and studied in conclusive, quantitative terms with the tools of numerical relativity. The following is a summary of our main results:

(i) We obtained a maximum final spin parameter equal to 1.00 for the WFF1, APR2, and PS nuclear equations of state, when using the mass ratio $M_{\rm BH}/M_{\rm NS} = 10$. $M_{\rm BH}/M_{\rm NS} = 2$ yields instead a maximum final spin parameter of 0.99. Given their absolute error of 0.02, these predictions are compatible with the 0.98 maximum found in [44] and provide indirect support to the cosmic censorship conjecture [94].

(ii) We discussed the dependence of $a_{\rm f}$ and $M_{\rm f}$ on the NS EOS, claiming that the EOS may leave an imprint on the BH remnant. The quasinormal mode frequency $f_{220}^{\rm QNM}$ of the BH remnant, which depends on $a_{\rm f}$ and $M_{\rm f}$ alone, could thus be used to constrain the NS EOS (Fig. 9). Deviations from the BH-BH values of $f_{220}^{\rm QNM}$ for symmetric mass ratios $\gtrsim 0.2$, with maximum deviations between $\sim$600 Hz and $\sim$1200 Hz. The excitation of the QNM oscillations does not occur for all mixed binary mergers, but it is likely to appear in the spectrum of the emitted gravitational radiation in the form of a cutoff frequency $f_{\rm cut} \simeq f_{220}^{\rm QNM}$ for systems with fairly compact NSs, i.e. for soft EOSs [44]. The possibility of constraining the EOS by measuring $f_{\rm cut} \simeq f_{220}^{\rm QNM}$ seems therefore complementary to other ideas for posing EOS constraints by means of GW detection, in that these favor constraints on stiff EOSs [13,15,44,96]. High-frequency gravitational waves from coalescing binaries may thus turn out to be, once more, very promising in terms of the NS EOS [97].

Future applications of the approach presented in this paper may be to exploit the predicted values of $a_{\rm f}$ and $M_{\rm f}$ to (1) provide the QNM frequencies to be used in the construction of hybrid waveforms for BH-NS systems [16,44], (2) develop phenomenological waveforms for BH-NS systems, (3) study time-frequency characteristics of the emitted radiation [61], and (4) build backgrounds for perturbative approaches to the study of the postmerger epoch. Two main extensions are, instead, foreseeable and consist in allowing for a more general initial state for the binary. One may investigate dropping the assumption that (1) the neutron star is initially irrotational and that (2) the initial spin angular momentum of the black hole and the orbital angular momentum are parallel. In the former case, one would have to add a spin angular momentum contribution from the neutron star to the numerator of Eq. (11) and allow for a fraction of this angular momentum to possibly be dissipated prior to the disruption/plunge of the star. A major obstacle, however, would be that, since there are no numerical-relativity simulations with a nonirrotational neutron star initial state, we lack a model to predict $M_{\rm b,torus}$ when the neutron star is initially spinning. As this quantity appears in Eq. (11), being able to predict it would be a fundamental gap to fill in, prior to extending the model discussed in this paper. Regarding cases with nonparallel black hole spin angular momentum and orbital angular momentum, the ISCO-related expressions appearing in Eq. (11) would have to be generalized. Input in this direction has recently started to emerge from the numerical-relativity community via the first simulations of tilted BH-NS mergers, e.g. [43], that would serve as test cases. In general, and independently of extending the model, it is important to keep testing the model as more numerical simulations are published in the literature, possibly constraining the ansatz of Eq. (12) and improving the model of [57], on which the entire approach relies.

In concluding this work, we would like to stimulate the BH-NS numerical-relativity community to continue investigating different parameter configurations, as this would allow us to better constrain the current version of our model [see the discussion following Eq. (11)]. Investigations on more generic initial spin configurations would also be helpful [43], as they would allow us to look into extending our approach.

ACKNOWLEDGMENTS

It is a pleasure to thank Emanuele Berti, John Friedman, Philipp Mösta, Frank Ohme, Luciano Rezzolla, and James Ryan for useful discussions and comments, and Tim Dietrich for carefully reading the manuscript. The author is grateful to the authors of [51] for testing the model discussed in this paper against their new results and validating it further. This work was supported in part by the DFG Grant SFB/Transregio 7.

APPENDIX: EQUATIONS OF STATE

NSs are the most compact objects known, lacking an event horizon. The densities in the interior of these stars are expected to exceed the equilibrium density of nuclear matter ($\rho_s \simeq 2.7 \times 10^{14}$ g/cm^{-3}), so their macroscopic properties, e.g. mass and radius, and the internal composition of their cores depend on the nature of strong interactions in dense matter and reflect (different aspects of) the dense matter EOS. Our knowledge about the behavior of

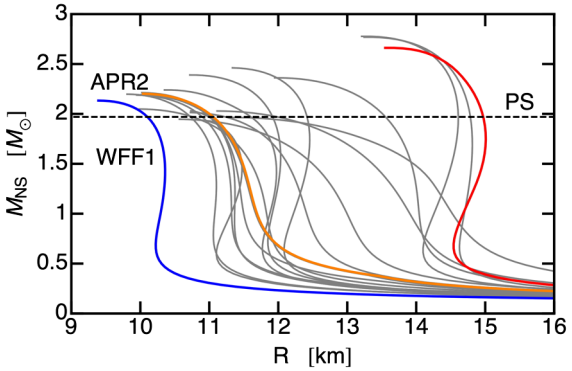

FIG. 10 (color online). NS equilibrium sequences in the radius-mass plane for several equations of state. The sequences shown are compatible with the recent measurement $M_{NS} = (2.01 \pm 0.04)M_\odot$ (horizontal, dashed line). Results for the WFF1/PS EOS, which yields the most/least compact NSs, are shown in blue/red. The APR2 sequence is shown in orange, while sequences obtained with other equations of state are shown with thinner, continuous gray lines.

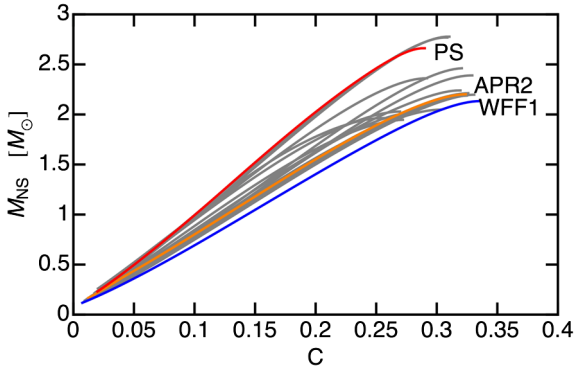

FIG. 11 (color online). Same as Fig. 10, but in the compactness-mass plane.

matter at such exceptionally high densities, however, is still currently limited. As far as the composition is concerned, for example, several dense matter models predict that—in addition to nucleons, electrons, and muons—exotica in the form of hyperons, a Bose condensate of mesons, or deconfined quark matter eventually appear at supranuclear densities [98].

An intense investigation to determine the EOS of dense matter was performed throughout the years [98–100]. The recent measurement of a NS with mass $M_{NS} = (2.01 \pm 0.04)M_\odot$ ruled out several equations of state proposed over time [89]. NS equilibrium sequences for EOSs[8] compatible with such measurement are shown in the radius-mass plane in Fig. 10. In order to assess the impact of the EOS on the BH remnant of BH-NS mergers, we pick the two EOSs that yield the smallest and the largest NS radii for any given NS mass between ~ 1 and $\sim 2.1M_\odot$. We dub these two EOSs WFF1 and PS, respectively, because of their NS core description [90,91]. The NS equilibrium sequences they yield are shown in blue and red in Fig. 10. As is obvious from the graph, the WFF1 and the PS EOS bracket all other equations of state in the relevant NS mass range[9] $1.0 \lesssim M_{NS}/M_\odot \lesssim 2.1$. The sequences of Fig. 10 are displayed in the compactness-mass plane in Fig. 11.

For both the WFF1 and the PS EOS, we use the same description of matter in the outer layers of the NS:

(i) for densities in the interval starting at the neutron drip density 4×10^{11} g/cm^3 and ending at 2×10^{14} g/cm^3, the Pethick-Ravenhall-Lorenz (PRL) EOS [102] is used;
(ii) for the crust layer in the density interval $(10^7 - 4 \times 10^{11})$ g/cm^3, the Baym-Pethick-Sutherland (BPS) EOS [103] is adopted;
(iii) and, finally, for densities lower than 10^7 g/cm^3 the BPS EOS is extrapolated.

The two EOSs differ at densities above 2×10^{14} g/cm^3: for the NS core we use what are strictly speaking the WFF1 EOS of [90] and the "liquid" version of the PS EOS of [91]. The WFF1 EOS for dense nuclear matter is based on a many-body Hamiltonian built with the Argonne v_{14} two-nucleon potential and the Urbana VII three-nucleon potential; calculations are performed with a variational method. The PS EOS, instead, considers neutron-only matter with π^0 condensates; the π^0 relativistic field is not treated explicitly but is instead replaced by an equivalent two-body potential; calculations are performed using a constrained variational method. Both WFF1 and PS are dated and have been superseded by more modern models and calculation techniques; however, they serve our purpose of considering extremely compact and extremely large NSs, respectively, to explore the space of parameters of BH-NS binaries.

In addition to the WFF1 and PS cases, we also discuss results obtained for the APR2 EOS [92], which is used as it represents the most complete nuclear many-body study to date, and special-relativistic corrections were progressively incorporated in it. APR2 is based on the Argonne v_{18} two-nucleon potential, the Urbana IX three-nucleon potential, and the δv_b boost; it is supported by current astrophysical [104] and nuclear physics constraints [105].

[8]We do not consider strange quark matter equations of state.
[9]The theoretical minimum mass for a proto-neutron star is 1.1–1.2$M_\odot$ [101].

[1] M. Shibata and K. Taniguchi, Living Rev. Relativity **14**, 6 (2011).
[2] V. Kalogera, K. Belczynski, C. Kim, R. O'Shaughnessy, and B. Willems, Phys. Rep. **442**, 75 (2007).
[3] K. Belczynski, R. E. Taam, V. Kalogera, F. Rasio, and T. Bulik, Astrophys. J. **662**, 504 (2007).
[4] K. Belczynski, R. E. Taam, E. Rantsiou, and M. van der Sluys, Astrophys. J. **682**, 474 (2008).
[5] R. O'Shaughnessy, C. Kim, V. Kalogera, and K. Belczynski, Astrophys. J. **672**, 479 (2008).
[6] J. Abadie, B. P. Abbott, R. Abbott, M. Abernathy, T. Accadia, F. Acernese, C. Adams, R. Adhikari, P. Ajith, B. Allen *et al.*, Classical Quantum Gravity **27**, 173001 (2010).
[7] LIGO: Laser Interferometer Gravitational Wave Observatory, http://www.ligo.caltech.edu/.
[8] Virgo, http://www.virgo.infn.it/.
[9] KAGRA: Kamioka Gravitational wave detector, http://gwcenter.icrr.u-tokyo.ac.jp/en/.
[10] M. Punturo *et al.*, Classical Quantum Gravity **27**, 084007 (2010).
[11] E. Nakar, Phys. Rep. **442**, 166 (2007).
[12] E. Berger, New Astron. Rev. **55**, 1 (2011).
[13] M. Vallisneri, Phys. Rev. Lett. **84**, 3519 (2000).
[14] V. Ferrari, L. Gualtieri, and F. Pannarale, Phys. Rev. D **81**, 064026 (2010).
[15] F. Pannarale, L. Rezzolla, F. Ohme, and J. S. Read, Phys. Rev. D **84**, 104017 (2011).
[16] B. D. Lackey, K. Kyutoku, M. Shibata, P. R. Brady, and J. L. Friedman, Phys. Rev. D **85**, 044061 (2012).
[17] J. M. Lattimer and D. N. Schramm, Astrophys. J. Lett. **192**, L145 (1974).
[18] B. D. Metzger and E. Berger, Astrophys. J. **746**, 48 (2012).
[19] K. Taniguchi, T. W. Baumgarte, J. A. Faber, and S. L. Shapiro, Phys. Rev. D **72**, 044008 (2005).
[20] P. Grandclément, Phys. Rev. D **74**, 124002 (2006).
[21] J. A. Faber, T. W. Baumgarte, S. L. Shapiro, and K. Taniguchi, Astrophys. J. **641**, L93 (2006).
[22] J. A. Faber, T. W. Baumgarte, S. L. Shapiro, K. Taniguchi, and F. A. Rasio, Phys. Rev. D **73**, 024012 (2006).
[23] A. A. Tsokaros and K. b. o. Uryū, Phys. Rev. D **75**, 044026 (2007).
[24] K. Taniguchi, T. W. Baumgarte, J. A. Faber, and S. L. Shapiro, Phys. Rev. D **75**, 084005 (2007).
[25] K. Taniguchi, T. W. Baumgarte, J. A. Faber, and S. L. Shapiro, Phys. Rev. D **77**, 044003 (2008).
[26] H.-T. Janka, T. Eberl, M. Ruffert, and C. L. Fryer, Astrophys. J. **527**, L39 (1999).
[27] M. Ruffert and H.-T. Janka, Astron. Astrophys. **344**, 573 (1999).
[28] W. Kluzniak and W. H. Lee, Astrophys. Lett. Commun. **38**, 205 (1999).
[29] S. Rosswog, Astrophys. J. **634**, 1202 (2005).
[30] F. Löffler, L. Rezzolla, and M. Ansorg, Phys. Rev. D **74**, 104018 (2006).
[31] C. F. Sopuerta, U. Sperhake, and P. Laguna, Classical Quantum Gravity **23**, S579 (2006).
[32] M. Shibata and K. Uryu, Phys. Rev. D **74**, 121503(R) (2006).
[33] M. Shibata and K. Uryu, Classical Quantum Gravity **24**, S125 (2007).
[34] Z. B. Etienne, J. A. Faber, Y. T. Liu, S. L. Shapiro, K. Taniguchi, and T. W. Baumgarte, Phys. Rev. D **77**, 084002 (2008).
[35] M. Shibata and K. Taniguchi, Phys. Rev. D **77**, 084015 (2008).
[36] E. Rantsiou, S. Kobayashi, P. Laguna, and F. A. Rasio, Astrophys. J. **680**, 1326 (2008).
[37] M. D. Duez, F. Foucart, L. Kidder, H. Pfeiffer, M. Scheel, and S. Teukolsky, Phys. Rev. D **78**, 104015 (2008).
[38] Z. B. Etienne, Y. T. Liu, S. L. Shapiro, and T. W. Baumgarte, Phys. Rev. D **79**, 044024 (2009).
[39] M. Shibata, K. Kyutoku, T. Yamamoto, and K. Taniguchi, Phys. Rev. D **79**, 044030 (2009).
[40] M. D. Duez, F. Foucart, L. E. Kidder, C. D. Ott, and S. A. Teukolsky, Classical Quantum Gravity **27**, 114106 (2010).
[41] K. Kyutoku, M. Shibata, and K. Taniguchi, Phys. Rev. D **82**, 044049 (2010).
[42] S. Chawla, M. Anderson, M. Besselman, L. Lehner, S. L. Liebling, P. M. Motl, and D. Neilsen, Phys. Rev. Lett. **105**, 111101 (2010).
[43] F. Foucart, M. D. Duez, L. E. Kidder, and S. A. Teukolsky, Phys. Rev. D **83**, 024005 (2011).
[44] K. Kyutoku, H. Okawa, M. Shibata, and K. Taniguchi, Phys. Rev. D **84**, 064018 (2011).
[45] K. Kyutoku, M. Shibata, and K. Taniguchi, Phys. Rev. D **84**, 049902 (2011).
[46] F. Foucart, M. D. Duez, L. E. Kidder, M. A. Scheel, B. Szilagyi, and S. A. Teukolsky, Phys. Rev. D **85**, 044015 (2012).
[47] Z. B. Etienne, Y. T. Liu, V. Paschalidis, and S. L. Shapiro, Phys. Rev. D **85**, 064029 (2012).
[48] M. Shibata, K. Kyutoku, T. Yamamoto, and K. Taniguchi, Phys. Rev. D **85**, 127502 (2012).
[49] Z. B. Etienne, V. Paschalidis, and S. L. Shapiro, Phys. Rev. D **86**, 084026 (2012).
[50] M. B. Deaton, M. D. Duez, F. Foucart, E. O'Connor, C. D. Ott, L. E. Kidder, C. D. Muhlberger, M. A. Scheel, and B. Szilagyi, arXiv:1304.3384v2.
[51] F. Foucart, M. B. Deaton, M. D. Duez, L. E. Kidder, I. MacDonald, C. D. Ott, H. P. Pfeiffer, M. A. Scheel, B. Szilagyi, and S. A. Teukolsky, Phys. Rev. D **87**, 084006 (2013).
[52] K. Kyutoku, K. Ioka, and M. Shibata, arXiv:1305.6309.
[53] F. Foucart, L. Buchman, M. D. Duez, M. Grudich, L. E. Kidder, I. MacDonald, A. Mroue, H. P. Pfeiffer, M. A. Scheel, and B. Szilagyi, arXiv:1307.7685.
[54] G. Lovelace, M. D. Duez, F. Foucart, L. E. Kidder, H. P. Pfeiffer, M. A. Scheel, and B. Szilágyi, Classical Quantum Gravity **30**, 135004 (2013).
[55] V. Paschalidis, Z. B. Etienne, and S. L. Shapiro, Phys. Rev. D **88**, 021504 (2013).
[56] M. Ruffert and H.-T. Janka, Astron. Astrophys. **514**, A66 (2010).
[57] F. Foucart, Phys. Rev. D **86**, 124007 (2012).
[58] M. Shibata, Prog. Theor. Phys. **96**, 917 (1996).
[59] P. Wiggins and D. Lai, Astrophys. J. **532**, 530 (2000).
[60] E. Berti, S. Iyer, and C. M. Will, Phys. Rev. D **77**, 024019 (2008).
[61] C. Hanna, M. Megevand, E. Ochsner, and C. Palenzuela, Classical Quantum Gravity **26**, 015009 (2009).
[62] V. Ferrari, L. Gualtieri, and F. Pannarale, Classical Quantum Gravity **26**, 125004 (2009).

[63] T. Damour and A. Nagar, Phys. Rev. D **81**, 084016 (2010).
[64] F. Pannarale, A. Tonita, and L. Rezzolla, Astrophys. J. **727**, 95 (2011).
[65] A. Buonanno and T. Damour, Phys. Rev. D **62**, 064015 (2000).
[66] T. Damour, Phys. Rev. D **64**, 124013 (2001).
[67] S. A. Hughes and R. D. Blandford, Astrophys. J. **585**, L101 (2003).
[68] A. Buonanno, Y. Chen, and T. Damour, Phys. Rev. D **74**, 104005 (2006).
[69] M. Campanelli, C. O. Lousto, and Y. Zlochower, Phys. Rev. D **73**, 061501 (2006).
[70] M. Campanelli, C. O. Lousto, and Y. Zlochower, Phys. Rev. D **74**, 041501 (2006).
[71] M. Campanelli, C. O. Lousto, and Y. Zlochower, Phys. Rev. D **74**, 084023 (2006).
[72] T. Damour and A. Nagar, Phys. Rev. D **76**, 044003 (2007).
[73] W. Tichy and P. Marronetti, Phys. Rev. D **76**, 061502 (2007).
[74] A. Buonanno, L. E. Kidder, and L. Lehner, Phys. Rev. D **77**, 026004 (2008).
[75] L. Rezzolla, E. N. Dorband, C. Reisswig, P. Diener, D. Pollney, E. Schnetter, and B. Szilágyi, Astrophys. J. **679**, 1422 (2008).
[76] L. Boyle, M. Kesden, and S. Nissanke, Phys. Rev. Lett. **100**, 151101 (2008).
[77] M. Kesden, Phys. Rev. D **78**, 084030 (2008).
[78] P. Marronetti, W. Tichy, B. Bruegmann, J. Gonzalez, and U. Sperhake, Phys. Rev. D **77**, 064010 (2008).
[79] L. Rezzolla, P. Diener, E. N. Dorband, D. Pollney, C. Reisswig, E. Schnetter, and J. Seiler, Astrophys. J. **674**, L29 (2008).
[80] L. Rezzolla, E. Barausse, E. N. Dorband, D. Pollney, C. Reisswig, J. Seiler, and S. Husa, Phys. Rev. D **78**, 044002 (2008).
[81] L. A. Gergely and P. L. Biermann, J. Phys. Conf. Ser. **122**, 012040 (2008).
[82] L. Rezzolla, Classical Quantum Gravity **26**, 094023 (2009).
[83] E. Barausse and L. Rezzolla, Astrophys. J. Lett. **704**, L40 (2009).
[84] M. Kesden, G. Lockhart, and E. S. Phinney, Phys. Rev. D **82**, 124045 (2010).
[85] E. Barausse, V. Morozova, and L. Rezzolla, Astrophys. J. **758**, 63 (2012).
[86] L. Bildsten and C. Cutler, Astrophys. J. **400**, 175 (1992).
[87] C. S. Kochanek, Astrophys. J. **398**, 234 (1992).
[88] E. Berti, V. Cardoso, and A. O. Starinets, Classical Quantum Gravity **26**, 163001 (2009).
[89] J. Antoniadis *et al.*, Science **340**, 448 (2013).
[90] R. B. Wiringa, V. Fiks, and A. Fabrocini, Phys. Rev. C **38**, 1010 (1988).
[91] V. R. Pandharipande and R. A. Smith, Nucl. Phys. A **237**, 507 (1975).
[92] A. Akmal and V. R. Pandharipande, Phys. Rev. C **56**, 2261 (1997); A. Akmal, V. R. Pandharipande, and D. G. Ravenhall, Phys. Rev. C**58**, 1804 (1998).
[93] L. Santamaría *et al.*, Phys. Rev. D **82**, 064016 (2010).
[94] R. Penrose, in *General Relativity: An Einstein Centenary Survey*, edited by S. Hawking and W. Israel (Cambridge University Press, Cambridge, England, 1979), p. 581.
[95] K. S. Thorne, Astrophys. J. **191**, 507 (1974).
[96] T. Hinderer, B. D. Lackey, R. N. Lang, and J. S. Read, Phys. Rev. D **81**, 123016 (2010).
[97] A. Bauswein, H.-T. Janka, K. Hebeler, and A. Schwenk, Phys. Rev. D **86**, 063001 (2012).
[98] J. M. Lattimer and M. Prakash, Phys. Rep. **442**, 109 (2007).
[99] M. Alford, Annu. Rev. Nucl. Part. Sci. **51**, 131 (2001).
[100] J. M. Lattimer and M. Prakash, Nucl. Phys. A **777**, 479 (2006).
[101] J. Goussard, P. Haensel, and J. L. Zdunik, Astron. Astrophys. **330**, 1005 (1998).
[102] C. J. Pethick, D. G. Ravenhall, and C. P. Lorenz, Nucl. Phys. A **584**, 675 (1995).
[103] G. Baym, C. Pethick, and P. Sutherland, Astrophys. J. **170**, 299 (1971).
[104] A. W. Steiner, J. M. Lattimer, and E. F. Brown, Astrophys. J. **722**, 33 (2010).
[105] K. Hebeler, J. M. Lattimer, C. J. Pethick, and A. Schwenk, Phys. Rev. Lett. **105**, 161102 (2010).